High-Resolution Gamma Spectrometry of a Plutonium Bearing Waste Drum With High-Energy Reaction-Induced Gamma Rays

V. Bottau, L. Tondut, P.-G. Allinei, B. Perot, C. Eleon, C. Carasco, R. De Stefano, and G. Faussier

***Abstract*— In the framework of the radioactive waste drum characterization using neutron coincidence counting, the Nuclear Measurement Laboratory of French Alternative Energies and Atomic Energy Commission (CEA) Cadarache is studying plastic scintillators as an alternative to ideal but costly ^{3}He gas proportional counters. Plastic scintillators are at least five times cheaper for the same detection efficiency, and in addition, they detect fast neutrons three orders of magnitude more quickly than ^{3}He detectors. However, they are sensitive to gamma rays with no pulse shape discrimination abilities for large detection volumes, which implies the necessity to identify precisely gamma background sources that may affect the useful signal. This article presents a detailed analysis of the gamma-ray spectrum of a radioactive waste drum containing glove box filters contaminated by plutonium dioxide. Classical gamma emissions following alpha and beta disintegrations are identified, and also those accompanying inelastic scattering (n, n′) or radiative capture (n, γ) reactions in the whole waste drum, and (α, n) or (α, p) reactions in the filtration media, which can lead to neutron-gamma coincidences parasitizing useful coincidences from plutonium spontaneous fissions.**

***Index Terms*— Gamma-ray spectrometry, high purity germanium detector (HPGe), plastic scintillators, plutonium dioxide, radioactive waste.**

I. Introduction

IN THE context of passive neutron measurements for nuclear material characterization, conventional coincidence collars based on ^{3}He gas counters permit temporal discrimination of spontaneous fission neutrons and parasitic neutrons from (α, n) reactions. ^{3}He proportional counters are the gold standard because they show a very high capture cross section for thermal neutrons, leading to high detection efficiency when surrounding detectors with polyethylene moderator, while being practically insensitive to gamma rays. However, the global shortage of ^{3}He gas [1] has greatly increased the cost in the past 15 years, leading to worldwide initiatives to look for cheaper alternatives with equivalent performances [2].

Manuscript received August 2, 2019; revised October 28, 2019; accepted November 29, 2019. Date of publication December 12, 2019; date of current version April 16, 2020. This work was supported by the CEA R&D program for radioactive waste characterization.

V. Bottau, P.-G. Allinei, B. Perot, C. Eleon, C. Carasco, and R. De Stefano are with French Alternative Energies and Atomic Energy Commission, Nuclear Energy Division, Cadarache, DTN, SMTA, Nuclear Measurement Laboratory, F-13108 Saint-Paul-lez-Durance, France (e-mail: vincent.bottau@cea.fr).

L. Tondut and G. Faussier are with Orano Business Unit Recycling, DT/E/MN/EXP, F-50440 La Hague, France.

Digital Object Identifier 10.1109/TNS.2019.2959079

The Nuclear Measurements Laboratory of French Alternative Energies and Atomic Energy Commission (CEA), Nuclear Energy Division (DEN), Cadarache, is currently studying the use of low-cost polyvinyl toluene (PVT) plastic scintillators as a potential alternative [3], [4] that have the advantage of being sensitive to fast neutrons, thus avoiding thermalizing materials and offering a nanosecond response time. Consequently, very short coincidence windows of a few tens of nanoseconds allow greatly reducing accidental coincidences compared to three orders of magnitude slower ^{3}He detection systems, mainly due to the time needed for neutron thermalization.

However, plastic scintillators are very sensitive to gamma rays. Some of them are emitted in coincidence with (α, n) neutrons often encountered with alpha bearing waste like those contaminated by plutonium and americium oxides, leading to neutron-gamma coincidences that penalize the detection of plutonium spontaneous fission coincidences. Other correlated gamma emissions may also occur in neutron-induced reactions, such as (n, n′) inelastic scattering. Pulse shape discrimination (PSD) liquid and plastic organic scintillators are commonly used to combat gamma sensitivity [5]–[11], but they would not constitute a cost-effective alternative to ^{3}He counters for large radioactive waste package characterization. Indeed, large detection solid angles and volumes are needed to preserve coincidence counting statistics and therefore, a large number of PSD scintillators should be implemented as their size is limited. Actually, the difference between neutron and gamma-ray pulse tails is not preserved in large PSD scintillators due to multiple light scattering [12], [13]. Finally, a large array of small (maximum 5 in) PSD scintillators would increase the cost to a similar level as ^{3}He detectors. In addition, PSD information lies in pulse tails and would be damaged by pulse pile-up in case of high count rate, as it is the case with some radioactive waste.

In view to find mitigations to gamma sensitivity of basic PVT plastic scintillators, this article reports the detailed gamma spectrum analysis of a 120-L waste drum containing glove box filters contaminated by plutonium dioxide powder. Classical gamma rays following the radioactive decays of americium and plutonium isotopes are identified, and also those emitted after (α, n) or (α, p) reactions in the filtration media, (n, n′) and (n, γ) reactions in the whole waste drum.

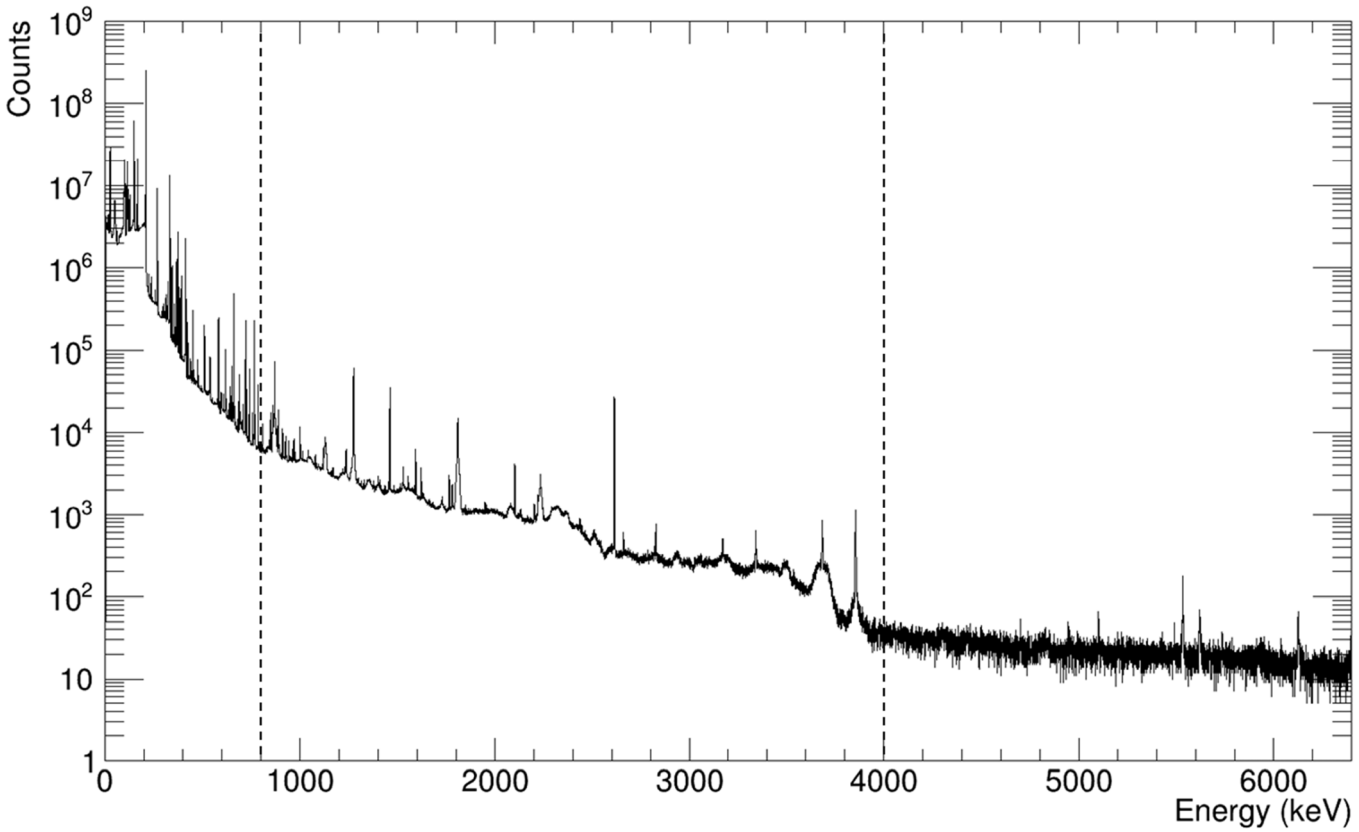

Fig. 1. Gamma spectrum of the 120-L plutonium waste drum resulting from a 38.7-h real-time measurement with a BEGe planar HPGe. The three main regions separated by dotted lines (from 0 to 800, 800 to 4000, and above 4000 keV) are analyzed in detail in Sections III-A–III-C.

TABLE I
ISOTOPIC COMPOSITION MEASURED

Radionuclide	MGA(% weight ± 1σ)
^{238}Pu	2.63 ± 0.83%
^{239}Pu	56.96 ± 0.74%
^{240}Pu	26.14 ± 1.06%
^{241}Pu	7.88 ± 0.80%
^{242}Pu	6.39 ± 10%
ratio ^{241}Am/Pu	1.47 ± 0.87%

TABLE II
GLOVE BOX FILTER COMPOSITION

Element	% weight
Si	27.53%
Al	2.52%
B	2.96%
Na	7.83%
K	1.84%
Ca	3.32%
Mg	0.71%
Fe	0.15%
Zn	2.51%
Ba	3.44%
F	1.03%
O	46.15%

II. EXPERIMENTAL SETUP

The high purity germanium (HPGe) detector used for the measurement is a planar broad energy germanium (BEGe) from Mirion Technologies (Canberra), equipped with a CP5 Cryo-Pulse. It was in quasi-contact with a 120-L radioactive waste drum containing glove box filters contaminated with plutonium dioxide (PuO_2).

Table I presents the isotopic composition measured with multigroup analysis (MGA) codes and Table II presents the mass composition of the filtration media on which the plutonium is deposited. These filters are contained in handles that are attached to a steel frame. Handles are made with polyethylene and thus contain hydrogen, but in an unknown quantity (not mentioned in Table II).

A 1-mm tin plate was placed in front of the detector to clean very low energy gamma rays from the spectrum, especially the very intense 59.5-keV line of ^{241}Am. The acquisition electronics is a Digital Signal Analyzer LX (DSALX) from Mirion-Canberra, including high-voltage, amplification, pulse digitization and processing, and gamma spectrum storage. Data acquisition and processing are performed with Genie2000 gamma spectrometry software from Mirion-Canberra. The measurement lasted over 53 h, from which 38.7 h of real acquisition time with a dead time of 27%. Registered pulses are coded on 16 384 channels and the resulting spectrum recorded on the [0–6400] keV range is given in Fig. 1.

III. SPECTRUM ANALYSIS

Three main regions of interest are as follows.

1) The well-known region below 800 keV with classical gamma rays following americium and plutonium decays.
2) A region between 800 and 4000 keV including gamma rays emitted by natural radionuclides (^{40}K, thorium and

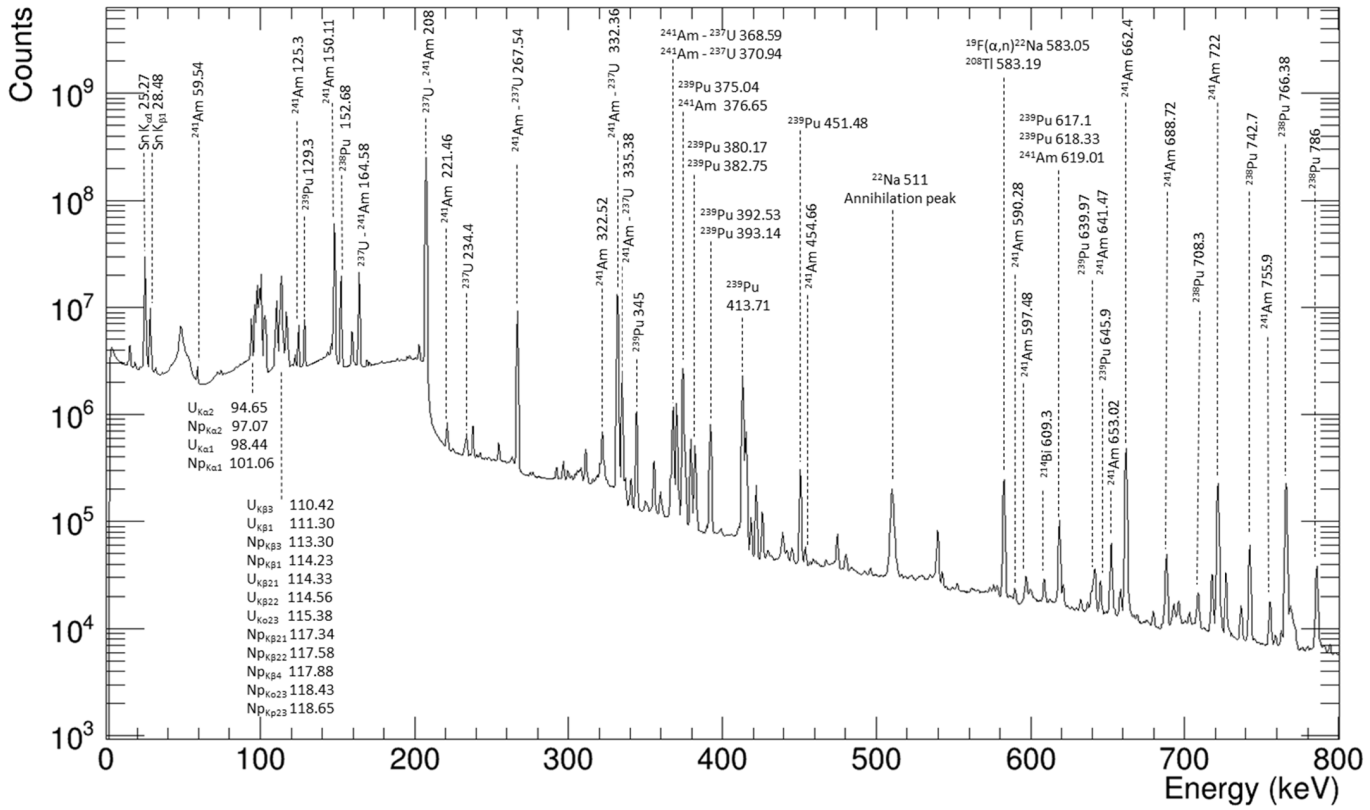

Fig. 2. X-rays and gamma rays from americium/plutonium in the 0–800-keV region of interest.

uranium chains), or accompanying (α, x) reactions on the light nuclei of oxygen (plutonium and americium oxides) and of the filtration media, or (n, n′) inelastic scattering reactions, or even radiative capture (n, γ). This region represents the very heart of this work because reaction gamma rays emitted in correlation with a neutron can lead to real but parasitic neutron-gamma coincidence, which are indistinguishable from useful spontaneous fission coincidences. In the case of (n, γ) reactions, crosstalk due to Compton scattering can also lead to spurious coincidences.

3) A region between 4000 and 6400 keV with few peaks due to neutron inelastic scattering which can, however, also generate parasitic neutron-gamma coincidence.

A. 0–800-keV Region of Interest

This region, for which a meticulous analysis has already been reported by Sampson [14], is highlighted in Fig. 2. It includes most of the gamma rays following radioactive disintegrations of ^{241}Am and plutonium isotopes. The two radioactive daughters of ^{241}Pu, ^{241}Am, and ^{237}U, are also present together with plutonium. Some of ^{237}U gamma rays are clearly visible (164.6, 208.0, 267.5, and 332.36 keV). Fig. 2 also shows the presence of many neptunium and uranium X-rays, ^{237}Np being produced by alpha decay of ^{241}Am and beta decay of ^{237}U. The excited ^{237}Np daughter nuclei return to ground state by emitting a large number of gamma and X-rays following internal conversion. ^{234}U, ^{235}U, and ^{236}U isotopes are produced from the alpha decay of ^{238}Pu, ^{239}Pu, and ^{240}Pu isotopes, leading also to many gamma and X-rays. ^{241}Pu (together with its ^{241}Am and ^{237}U daughters) is the major contributor to the low-energy part of the spectrum (up to the 335.38-keV peak), followed by ^{239}Pu and ^{238}Pu. With a long half-life of 373×10^3 years and small intensity gamma or X-rays, ^{242}Pu has no visible signature on the spectrum.

B. 800–4000-keV Region of Interest

Figs. 3 and 4 show the spectrum in the 800–1900- and 1900–4000-keV ranges, respectively. Tables III and IV give the intensity and the emitter of each identified gamma ray. Fig. 3 also shows many signatures from the ^{232}Th natural decay chain, notably from ^{228}Ac, ^{212}Bi, and ^{208}Tl. The ^{228}Ac radionuclide shows many peaks at 911, 965, 969, 1495, 1588, and 1631 keV. The gamma rays of ^{212}Bi (1079 and 1513 keV) and ^{208}Tl (861-keV line, 2614 keV plus its single escape (SE) and double escape (DE) peaks) are also clearly detected. From the ^{238}U natural decay chain, seven signatures of ^{214}Bi are also visible at 1120, 1408, 1509, 1661, 1730, 1764, and 2204 keV, in addition to the 609-keV gamma ray clearly visible on Fig. 2. Finally, the classical 1461-keV gamma ray of natural ^{40}K is also present.

In addition to the above classical lines, the 800–4000-keV region also shows less common gamma rays originating from alpha and neutron-induced reactions, which are of high importance for our neutron-gamma coincidence measurements

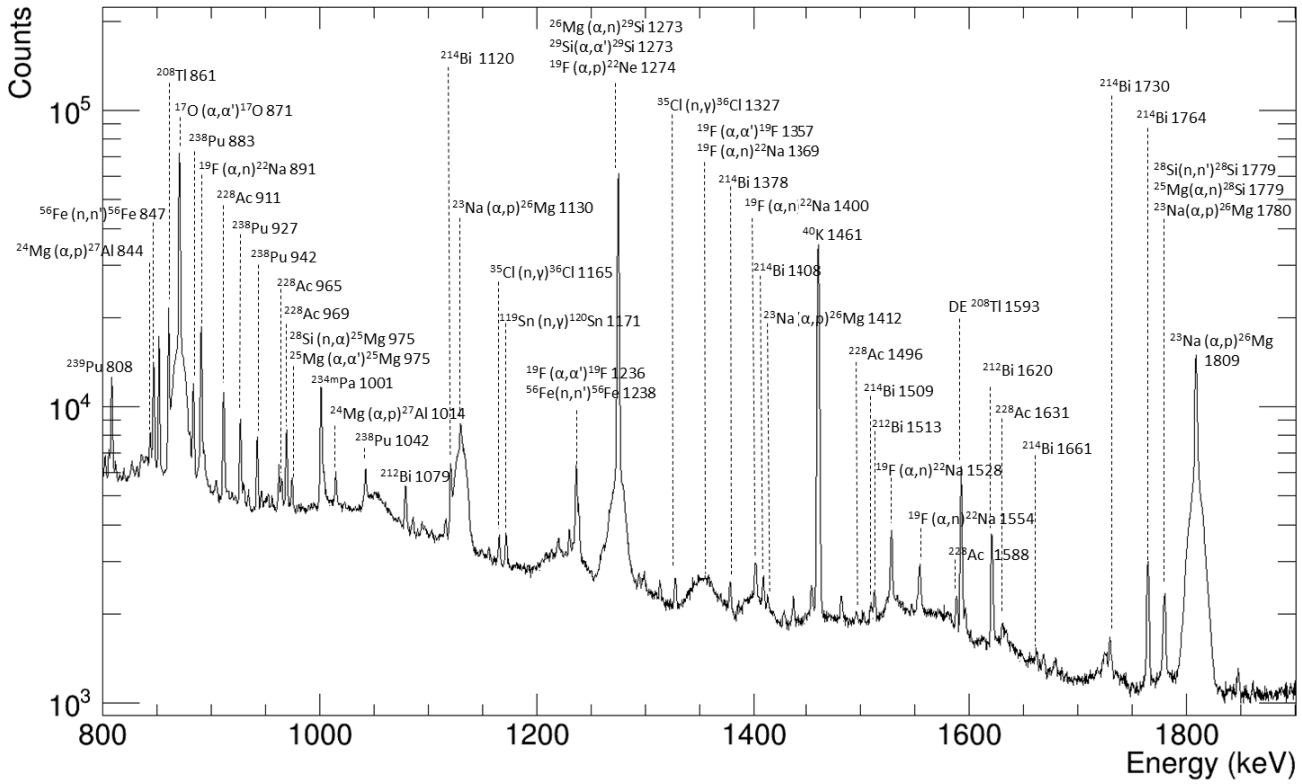

Fig. 3. Gamma rays from natural radionuclides (^{40}K, ^{238}U, and ^{232}Th decay chains), (α, x), (n, γ), and (n, n′) reactions in the 800–1900-keV energy range.

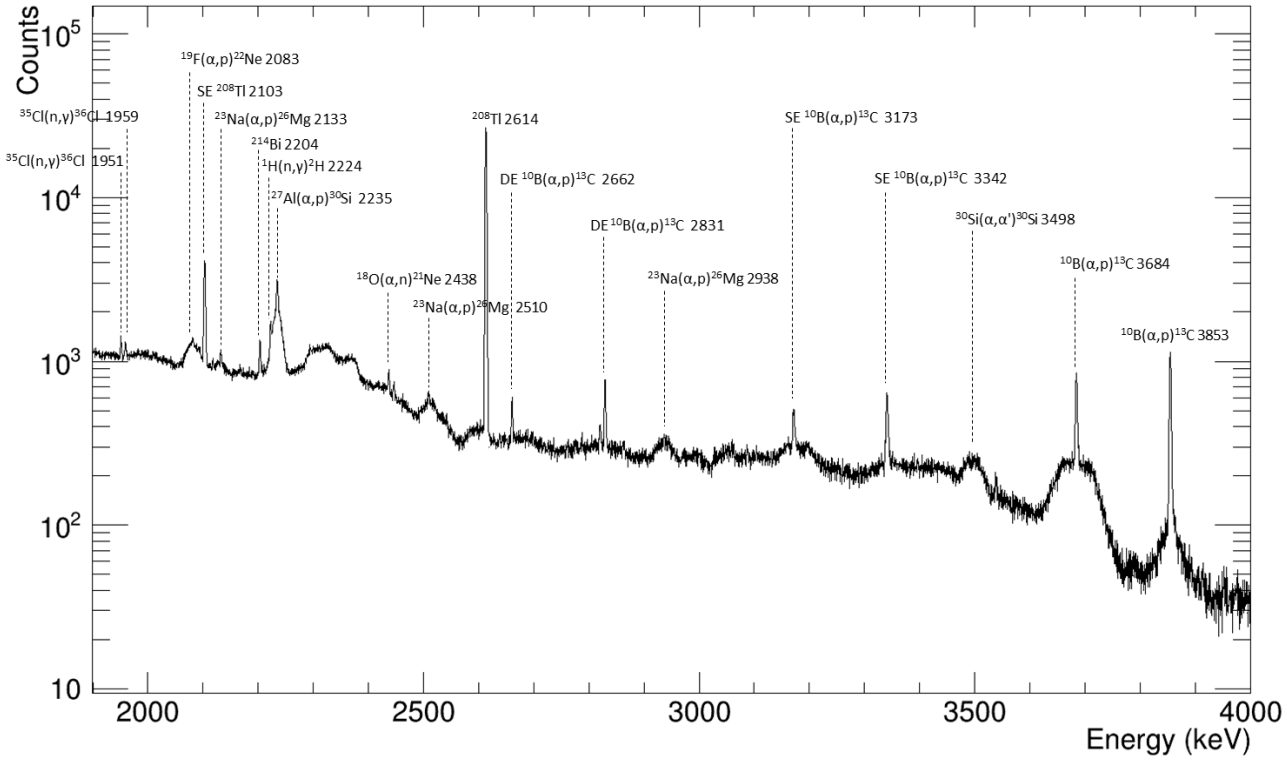

Fig. 4. Gamma rays from natural radionuclides (^{238}U and ^{232}Th decay chains), (α, x), (n, γ) and (n, n′) reactions in the 1900–4000 keV energy range. Broadened peaks around 2330 and 2370 keV remain to be identified and are prospected.

with plastic scintillators. Excited states of reaction product nuclides have been analyzed to propose potential reactions that can lead to the observed gamma rays. Energy levels and gamma-ray transitions are taken from the Evaluated Nuclear Structure Data File (ENSDF) [15]. Cross sections of (α, x) reactions were calculated with EMPIRE-II v.2.18 code [16] developed by the International Atomic Energy Agency (IAEA), considering 5.5-MeV alpha particles. Cross sections

TABLE III
PEAK ENERGIES AND BRANCHING RATIO IN 800–1900-keV RANGE

Original nuclide	Energy (keV)	Intensity (%) or Cross section (mbarn)	Reaction or radioactive daughter
^{24}Mg	843.76	17.8 mb	^{24}Mg(α,p)^{27}Al
^{56}Fe	846.764	621 mb	(n,n') ^{56}Fe
^{208}Tl	860.564	1.242×10^{1}	^{208}Pb
^{17}O	870.71	19.1 mb	(α,α') ^{17}O
^{238}Pu	883.240	7.700×10^{-7}	^{234}U
^{19}F	890.87	24.4 mb	(α,n) ^{22}Na
^{228}Ac	911.204	2.580×10^{1}	^{228}Th
^{238}Pu	926.720	5.800×10^{-7}	^{234}U
^{238}Pu	941.940	4.700×10^{-7}	^{234}U
^{228}Ac	964.766	4.990×10^{0}	^{228}Th
^{228}Ac	968.971	1.580×10^{1}	^{228}Th
^{25}Mg	974.742	0.924 mb	(α,α') ^{25}Mg
^{24}Mg	974.742	53.7 mb	(n,γ) ^{25}Mg
^{28}Si	974.742	41 mb	(n,α) ^{25}Mg
^{234m}Pa	1001.030	8.370×10^{-1}	^{234}U
^{24}Mg	1014.52	22.8 mb	(α,p) ^{27}Al
^{238}Pu	1041.700	2.200×10^{-7}	^{234}U
^{212}Bi	1078.620	5.640×10^{-1}	^{212}Po
^{214}Bi	1120.287	1.510×10^{1}	^{214}Po
^{23}Na	1129.61	44.3 mb	(α,p) ^{26}Mg
^{35}Cl	1164.860	43840 mb (total)	(n,γ) ^{36}Cl
^{119}Sn	1171.25	1135 mb (total)	(n,γ) ^{120}Sn
^{19}F	1235.8	27.97 mb	(α,α') ^{19}F
^{56}Fe	1238.274	290 mb	(n,n') ^{56}Fe
^{26}Mg	1273.361	76.5 mb	(α,n) ^{29}Si
^{29}Si	1273.361	1.13 mb	(α,α') ^{29}Si
^{19}F	1274.537	80.7 mb	(α,p) ^{22}Ne
^{35}Cl	1327.40	43840 mb (total)	(n,γ) ^{36}Cl
^{19}F	1356.9	17.466 mb	(α,α') ^{19}F
^{19}F	1368.7	24 mb	(α,n) ^{22}Na
^{214}Bi	1377.669	4.000×10^{0}	^{214}Po
^{19}F	1400.4	16.6 mb	(α,n) ^{22}Na
^{214}Bi	1407.980	2.150×10^{0}	^{214}Po
^{23}Na	1411.72	4.85 mb	(α,p)^{26}Mg
^{40}K	1460.830	1.100×10^{1}	^{40}Ar
^{228}Ac	1495.930	8.600×10^{-1}	^{228}Th
^{214}Bi	1509.228	2.110×10^{0}	^{214}Po
^{212}Bi	1512.700	2.900×10^{-1}	^{212}Po
^{19}F	1528.1	9.54 mb	(α,n)^{22}Na
^{19}F	1554.4	12.7 mb	(α,n)^{22}Na
^{228}Ac	1588.190	3.220×10^{0}	^{228}Th
^{208}Tl	1592.533	-	^{208}Pb (DE 2614.533)
^{212}Bi	1620.500	1.490×10^{0}	^{212}Po
^{228}Ac	1630.627	1.510×10^{0}	^{228}Th
^{214}Bi	1661.280	1.150×10^{0}	^{214}Po
^{214}Bi	1729.595	2.920×10^{0}	^{214}Po
^{214}Bi	1764.494	1.540×10^{1}	^{214}Po
^{28}Si	1778.969	403 mb	(n,n') ^{28}Si
^{25}Mg	1778.969	114 mb	(α,n) ^{28}Si
^{23}Na	1779.74	4.33 mb	(α,p)^{26}Mg
^{23}Na	1808.68	123 mb	(α,p)^{26}Mg

of fast neutron-induced reactions are taken from [17], where experimental data have been reported for 14.5-MeV neutrons. Cross sections for thermal neutron radiative capture and corresponding gamma-ray energies are taken from [18].

The following list, in the order of increasing atomic number of the target nuclei or excited reaction daughters (e.g., ^{13}C, ^{22}Na, and ^{26}Mg), reports capture gamma rays and gamma transitions of (α, x) and (n, n$'$) reaction products that possibly correspond to gamma rays observed in the spectrum.

1) The well-known 2223-keV gamma ray from thermal neutron radiative capture by ^{1}H [18] is clearly visible in the spectrum, hydrogen being present in plastic handles in which the glove box filters are conditioned.

TABLE IV
PEAK ENERGIES AND BRANCHING RATIO IN 1900–4000-keV RANGE

Original nuclide	Energy (keV)	Intensity (%) or Cross section (mbarn)	Reaction or radioactive daughter
^{35}Cl	1951.126	43840 mb (total)	(n,γ) ^{36}Cl
^{35}Cl	1959.337	43840 mb (total)	(n,γ) ^{36}Cl
^{19}F	2082.7	17 mb	(α,p) ^{22}Ne
^{208}Tl	2103.533	-	^{208}Pb (SE 2614.5)
^{23}Na	2132.71	6.30 mb	(α,p) ^{26}Mg
^{214}Bi	2204.220	5.080×10^{0}	^{214}Po
^{1}H	2223.248	332.6 mb	(n,γ) ^{2}H
^{27}Al	2235.23	67.6 mb	(α,p) ^{30}Si
^{18}O	2437.84	31.1 mb	(α,n) ^{21}Ne
^{23}Na	2510.01	9.52 mb	(α,p) ^{26}Mg
^{208}Tl	2614.533	9.90×10^{1}	^{208}Pb
^{10}B	2661.921	-	(α,p) ^{13}C (DE 3683.921)
^{10}B	2831.170	-	(α,p) ^{13}C (DE 3853.170)
^{23}Na	2938.15	4.92 mb	(α,p) ^{26}Mg
^{10}B	3172.921	-	(α,p) ^{13}C (SE 3683.921)
^{10}B	3342.170	-	(α,p) ^{13}C (SE 3853.170)
^{27}Al	3498.33	10.8 mb	(α,p) ^{30}Si
^{10}B	3683.921	45.9 mb	(α,p) ^{13}C
^{10}B	3853.170	30.5 mb	(α,p) ^{13}C

TABLE V
MOST INTENSE GAMMA RAYS FROM ^{21}Ne DE-EXCITATION. I_{rel} IS THE RELATIVE INTENSITY. THE HALF TIME GIVEN CORRESPONDS TO THE ORIGINAL LEVEL OF EACH TRANSITION

Energy (keV)	Transition	$T_{1/2}$ (fs)	I_{rel} (%)
350.725(3)	350.727(5/2+) → 0 (3/2+)	7130	100
1395.131(2)	1745.910(7/2+) → 350.727 (5/2+)	52	100
2437.84(1)	2788.79(1/2-) → 350.727 (5/2+)	81	100
2793.94(3)	2794.17(1/2+) → 0 (3/2+)	5.5	100
1120.0(2)	2866.6(9/2+) → 1745.910 (7/2+)	40	100
3311.92(3)	3663.57(3/2-) → 350.727 (5/2+)	65	100

(1) Identified in the spectrum
(2) Supposedly present but interfered by more intense peaks or masked in the continuum
(3) Unobserved

2) Two intense gamma rays corresponding to transitions from the two and three excited levels of ^{13}C (produced by (α, p) reaction on ^{10}B as boron are present in the filtering media) to the ground state and are visible in Fig. 4 [19]. These two lines are 3684 keV [3684.507 (3/2$^-$) → 0 (1/2$^-$)] and 3853 keV [3853.807 (5/2$^+$) → 0 (1/2$^-$)]. Large Doppler energy broadening is observed for the 3684-keV peak because the short lifetime of the excited state (half-life of 1.10 fs) allows gamma ray de-excitation while the residual ^{13}C nucleus is still slowing down. The Stopping and Range of Ions in Matter (SRIM) [20] calculation indeed shows that the slowing down of a ^{13}C nucleus is typically hundreds of femtoseconds. The shorter the excited state lifetime, the larger the broadening effect, as can be seen with the 3853-keV gamma ray, for which the de-excitation of the 3853.807-keV level (half-life of 8.60 ps) induces a smaller broadening. The 3089-keV gamma ray corresponding to the transition from the first excited state of ^{13}C to the ground state was also expected but is not identifiable in Fig. 4, probably due to an expected large Doppler broadening (1.07-fs lifetime of the first excited level).
3) The transition between the first excited state and the ground state of ^{17}O [870.73 (1/2$^+$) → 0 (5/2$^+$)] leads to an 871-keV gamma ray [21] visible in the spectrum. Due to the long lifetime of this first excited level (179 ps), no Doppler effect should be observed but the base of the peak is clearly broadened. This might be due to another unidentified broadened transition close to 870 keV. This gamma ray might be produced by inelastic scattering of alpha or neutron particles on ^{17}O nuclei. However, as ^{17}O is the least abundant isotope of oxygen (0.038%), the (n, n′) production mode is negligible because only elements with a minimum weight proportion of a few percent can lead to detectable fast neutron-induced gamma rays [22]. Conversely, the (α, α') reaction on ^{17}O is more probable. Tilley *et al.* [21] indicate that the excited state at 870.73 keV is the only reachable level by alpha inelastic scattering on ^{17}O nuclei. Therefore, the 2184-keV gamma ray from [3055.36 (1/2$^-$) → 870.73 (1/2$^+$)] transition does not appear in the spectrum, neither the 3842-keV gamma ray from [3842.8 (5/2$^-$) → 0 (5/2$^+$)] transition.
4) The transition [1345.67 (5/2$^-$) → 109.894 (1/2$^-$)] between ^{19}F excited levels [23] leads to a 1236-keV gamma ray identified in Fig. 3. In addition, a very broad "peak" corresponding to the 1357-keV gamma ray (in fact, the line is no more visible due to large Doppler broadening) from the [1554.038 (3/2$^+$, 3.5 fs) → 197.143 (5/2$^+$)] transition is also present. The production reaction leading to excited ^{19}F is probably alpha inelastic scattering on ^{19}F nuclei, as fluorocarbon is present in the filters. The ^{16}O(α, p) reaction could also lead to ^{19}F nuclei but is not possible with 5.5-MeV alpha particles. The transitions between the [109.894 (1/2$^-$) → 0 (1/2$^+$)] and [197.143 (5/2$^+$) → 0 (1/2$^+$)] ^{19}F excited levels should also lead to low-energy gamma rays, but in this energy region they are masked by the

TABLE VI

MOST INTENSE GAMMA RAYS FROM ^{22}Na DE-EXCITATION. I_{rel} IS THE RELATIVE INTENSITY. THE HALF TIME GIVEN CORRESPONDS TO THE ORIGINAL LEVEL OF EACH TRANSITION

Energy (keV)	Transition	$T_{1/2}$ (fs)	I_{rel} (%)
583.04(2)	583.05 (1+) → 0 (3+)	2.43×10^{8}	100
73.9(3)	657.00 (0+) → 583.05 (1+)	1.96×10^{4}	100
890.87(1)	(890.89 (4+) → 0 (3+)	10^{4}	100
1528.1(1)	1528.1 (5+) → 0 (3+)	3.42×10^{3}	100
1280.5(2)	1936.9 (1+) → 657 (0+)	1.3×10^{1}	100
1368.7(2)	1951.8 (2+) → 583.05 (1+)	8	100
1400.4(1)	1983.5 (3+) → 583.05 (1+)	1.47×10^{3}	100
1554.4(1)	2211.3 (1-) → 657 (0+)	1.49×10^{4}	100

(1) Identified in the spectrum
(2) Supposedly present but interfered by more intense peaks or masked in the continuum
(3) Unobserved

TABLE VII

MOST INTENSE GAMMA RAYS FROM ^{26}Mg DE-EXCITATION. I_{rel} IS THE RELATIVE INTENSITY. THE HALF TIME GIVEN CORRESPONDS TO THE ORIGINAL LEVEL OF EACH TRANSITION

Energy (keV)	Transition	$T_{1/2}$ (fs)	I_{rel} (%)
1808.68(1)	1808.74 (2+) → 0 (0+)	476	100
1129.61(1)	2938.33 (2+) → 1808.74 (2+)	141	100
2938.15(1)	2938.33 (2+) → 0 (0+)	141	10.7
1779.74(1)	3588.56 (0+) → 1808.74 (2+)	6450	100
1003.25(2)	3941.57 (3+) → 2938.33 (2+)	830	100
2132.71(1)	3941.57 (3+) → 1808.74 (2+)	830	61.3
2510.01(1)	4318.89 (4+) → 1808.74 (2+)	272	100
2523.69(3)	4332.52 (2+) → 1808.74 (2+)	20	100
1411.72(1)	4350.09 (3+) → 2938.33 (2+)	105	93
2541.18(3)	4350.09 (3+) → 1808.74 (2+)	105	100
1896.72(3)	4835.13 (2+) → 2938.33 (2+)	28	100

(1) Identified in the spectrum
(2) Supposedly present but interfered by more intense peaks or masked in the continuum
(3) Unobserved

intense gamma emissions following radioactive decays of americium and plutonium isotopes. However, it is worth noting that the transitions of 1236- and 1357-keV gamma rays populate the 197.143- and 109.894-keV levels, respectively, therefore leading to possible gamma coincidences bringing an additional correlated background in our foreseen plutonium measurement with plastic scintillators. Finally, the 2583-keV gamma ray (100% relative intensity) from the [2779.849 ($9/2^+$, 194 fs) → 197.143 ($5/2^+$)] transition, probably with a large Doppler effect, is not visible.

5) The 2438-keV gamma ray of ^{21}Ne [24] is visible in Fig. 4. Table V gives the six most intense de-excitation gamma rays of this nucleus. The 351-keV gamma ray is not visible because it is masked by americium and plutonium gamma emissions. The 1120- and 1395-keV gamma rays may also be present, but the ^{214}Bi gamma ray at 1120 keV, on the one hand, and the broadened peak at 1400 keV from ^{22}Na (as explained below), on the other hand, prevent from identifying them. Oxygen is very abundant in the waste and ^{21}Ne is probably produced by (α, n) reactions on ^{18}O (0.205% abundance in oxygen). Alpha radiative capture by ^{17}O can also lead to 351-, 1120-, and 1395-keV gamma rays, but not to the 2438 keV one because the 2788.79-keV excited state of ^{21}Ne cannot be reached by this reaction.
6) Two gamma rays corresponding to the first two excited levels of ^{22}Ne are identified. Excited ^{22}Ne nuclei probably come from (α, p) reactions on ^{19}F, as fluorine is present in the composition of the glove box filters constituting the waste. The transitions from the first excited state to the ground state [1274.537 (2^+) → 0 (0^+)] and from the two to one excited states [3357.2 (4^+) → 1274.537 (2^+)] of ^{22}Ne lead respectively to the 1274 keV (Fig. 3) and 2083 keV (Fig. 4) gamma rays [25]. Both peaks show Doppler broadening, which is consistent with the short lifetime of the 3357.2-keV level (225 fs) for the 2082-keV peak, but not with the longer lifetime (3600 fs) of 1274.537-keV level for the 1274-keV peak. Doppler broadening is probably due to another nuclear reaction, discussed later in this article, producing the ^{29}Si first excited level with a short lifetime (291 fs) and leading to a 1273-keV gamma ray.
7) Among the first height most intense (100% of relative intensity) de-excitation gamma rays given in Table VI for ^{22}Na [25], four are observed on the spectrum: 891, 1400, 1528, and 1554 keV. The 583-keV gamma ray is interfered by the 583-keV gamma ray of ^{208}Tl, and the 74 keV is masked by the intense americium and plutonium signal. The 1280 keV is probably drowned in the very intense broadened peak at 1274 keV, which is also contributed by the beta decay of ^{22}Na. Concerning the 1369-keV peak, because of the very short half-life of the 1951.8-keV level (8 fs), an important broadening is expected and might be responsible for the fact that this gamma ray is not clearly identifiable in Fig. 3. However, a broad bump is clearly present, probably merged with the broad peak of ^{19}F at 1357 keV mentioned earlier. The ^{22}Na excited state probably comes from the (α, n) reaction on ^{19}F. The 511-keV annihilation shown in Fig. 2 is a signature of the beta decay of generated ^{22}Na nuclei.
8) The 975-keV peak visible in Fig. 3 is assigned to the [974.756 ($3/2^+$) → 0 ($5/2^+$)] transition of ^{25}Mg [26] produced by (n, α) reaction on ^{28}Si. Indeed, silicon is a major constituent of the waste (see Table II) and ^{28}Si presenting a 92 % abundance. On the other hand, magnesium is present in the filter waste composition but in limited weight fraction (0.71%, see Table II), ^{25}Mg has only a 10% isotopic abundance, and neutron inelastic scattering could only be a minor production mode. In case of sufficient neutron thermalization in the waste, radiative capture by ^{24}Mg (79% isotopic abundance in magnesium) might also be a way to produce excited ^{25}Mg nuclei, but with a very small cross section of 53.7 mb [18] making this production negligible too. Nuclear data for ^{25}Mg energy levels and gamma transitions show that the 585 keV (100% of relative intensity) and 1611 keV (100% of relative intensity) gamma rays should also be present in the

TABLE VIII
NUCLEAR DATA OF THE NINE MOST INTENSE GAMMA RAYS FROM ^{30}Si DE-EXCITATION

Energy (keV)	Transition	$T_{1/2}$ (fs)	I_{rel} (%)
2235.23(1)	2235.322 (2+) → 0 (0+)	215	100
1263.13(2)	3498.49 (2+) → 2235.322 (2+)	58	100
3498.33(1)	3498.49 (2+) → 0 (0+)	58	98
1534.12(3)	3769.48 (2+) → 2235.322 (0+)	36	100
3769.22(3)	3769.48 (2+) → 0 (0+)	36	85
1552.36(3)	3787.72 (0+) → 2235.322 (0+)	8300	100
1311.80(3)	4810.31 (2+) → 3498.49 (2+)	104	89
2595.39(2)	4830.85 (3+) → 2235.322 (0+)	83	100
1732.7(3)	5231.38 (3+) → 3498.49 (2+)	43	100
3043.2(3)	5279.37 (4+) → 2235.322 (0+)	83	100

(1) Identified in the spectrum
(2) Supposedly present but interfered by more intense peaks or masked in the continuum
(3) Unobserved

spectrum [26]. However, the first one is in interference with the 583-keV peak of ^{208}Tl, and the second one comes from an excited state with a very short half-life [1611.768 keV ($7/2^+$, 17 fs)] potentially leading to large Doppler broadening detrimental to its detection.

9) Several gamma signatures from ^{26}Mg are observed. The main gamma transitions of this isotope are given in Table VII [27]. Excited levels of ^{26}Mg can be produced by (α, p) reactions on ^{23}Na nuclei present in the waste. On the contrary, neutron inelastic scattering on ^{26}Mg is probably negligible as this isotope abundance is only 11% of magnesium, this last representing a small mass fraction (0.71%) of the waste composition. Seven gamma rays given in Table VII are visible on the spectrum. Most of these are due to transitions toward the 1808.74-keV first excited level, which explains the high intensity of the 1809 keV that is also largely Doppler broadened due to its short half-life (476 fs). These cascades of gamma transitions temporally correlated with the 1809-keV gamma ray will again lead to parasitic coincidence with respect to spontaneous fission coincidences in plastic scintillators. The 1003-keV gamma ray interferes with the well-known ^{234m}Pa gamma ray at 1001 keV (^{238}U chain), but it seems to be present on the right side of this peak. The 1130- and 2938-keV gamma rays, coming from the same excited level at 2938.33 keV with a short half-life (141 fs), present a large energy broadening by Doppler effect. A lower relative intensity and a weaker detection efficiency for the 2938.15-keV gamma ray, compared to 1129.61-keV gamma ray, lead to the fact that only the broadening around 2938 keV is identifiable on Fig. 4. The 1780-keV transition is also visible in Fig. 3, but other reactions leading to excited ^{28}Si can also contribute at 1779 keV, as discussed in the following. Excited levels that can be populated, such as 2938.33-, 4318.89-, or 4350.09-keV levels, may induce a correlation between several gamma rays. For example, an (α, p) reaction leading to the 4350.09-keV excited state of ^{26}Mg can induce a correlated gamma cascade with the 1412-, 1130-, and 1809-keV gamma rays, and subsequently to coincidence possibly disturbing spontaneous fission coincidence counting. On the other hand, the 1897-, 2524-, and 2541-keV gamma rays reported in Table VII are not identified on the spectrum (see Fig. 4).

10) The 844- and 1014-keV gamma rays (both with a 100% relative intensity) visible in Fig. 3 are characteristic of ^{27}Al [28]. The 2212-keV transition (100% relative intensity) expected for this excited nuclei is not visible because of the proximity to the broadened 2235-keV peak due to ^{27}Al(α, p)^{30}Si, as detailed further. The ^{27}Al excited nuclei come from (α, p) reactions on ^{24}Mg, which has a 79% isotopic abundance in natural magnesium. Alpha radiative capture on ^{23}Na or alpha inelastic scatterings are discarded because of very low cross sections (respectively $\sim 10^{-2}$ and 1 mb) compared to (α, p) cross section ($\sim$20 mb) given in Table III. Furthermore, excited states responsible for these observed gamma rays cannot be populated by inelastic scattering of 5.5-MeV alpha particles [28].

11) A single transition of 1779 keV from the first excited state of ^{28}Si (1779.030 (2+), 475 fs of half-life) to the ground state [29] is identified in Fig. 3. The excited ^{28}Si nuclei is produced by neutron inelastic scattering on ^{28}Si (92.2% isotopic abundance in silicon) or (α, p) reaction on ^{25}Mg. As mentioned earlier, the 1779-keV line is in interference with the 1780-keV gamma ray due to^{23}Na(α, p)^{26}Mg reaction.

12) The 1273-keV gamma ray from the transition between the first excited state [1273.387 (3/2+)] and the ground state (1/2+) of ^{29}Si [30] is present in Fig. 3. Radiative capture on ^{28}Si (92.2% isotopic abundance) and inelastic scattering on ^{29}Si (4.7% abundance) can lead to excited ^{29}Si, as well as ^{26}Mg(α, n) and ^{29}Si(α, α') reactions. The 1273-keV peak shows significant Doppler broadening due to the short half-life (291 fs) of the 1273.387-keV excited level. It is worth reminding that this peak is very close to the already quoted 1274-keV gamma ray of ^{22}Ne. As mentioned earlier, this last is not Doppler broadened, in principle, due to the long half-life of its original ^{22}Ne excited level, and therefore broadening only comes from the ^{29}Si level.

13) Two gamma rays of ^{30}Si are identified in Fig. 4 at 2235 keV, from the first excited level (215 fs) to the ground state, and 3498-keV gamma ray from the second excited level (58 fs) to the ground state [31] (see Table VIII). Both are logically Doppler broadened due to the short lifetimes of their original excited levels, especially the 3498-keV gamma ray for which the full energy peak is not even visible. The 1263-keV gamma transition is almost completely drowned in the intense and broadened 1274-keV peak, but it might be guessed on the left tail. The 2595-keV transition originating from the 4830.84-keV level (83 fs) is expected to be very broadened and seems to be present on the left tail of the intense 2614.533-keV peak of ^{208}Tl. Other transitions presented in Table VIII are not observable on the spectrum, most of them being expected with large Doppler

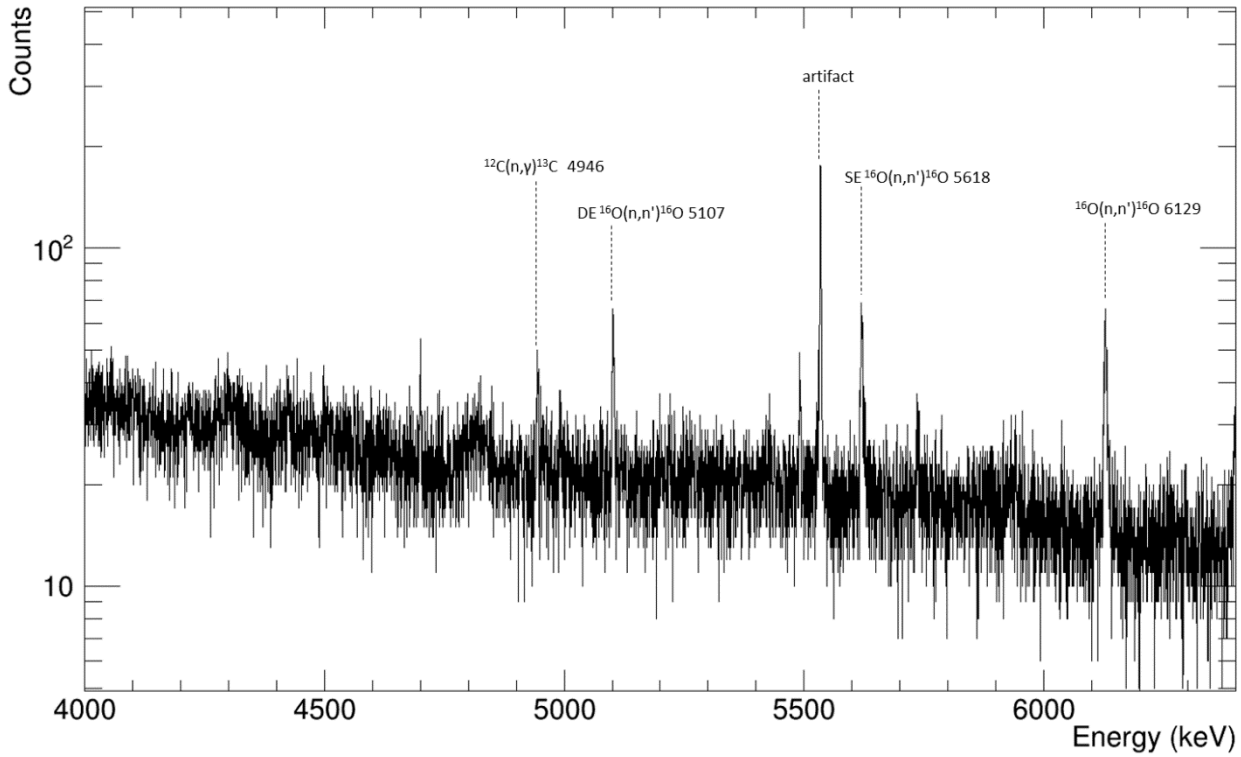

Fig. 5. Gamma rays from neutron radiative capture and inelastic scattering reactions in the high-energy range (4000–6400 keV).

TABLE IX
NUCLEAR DATA OF THE NINE MOST INTENSE GAMMA RAYS FROM ^{36}Cl DE-EXCITATION

Energy (keV)	Transition	$T_{1/2}$ (fs)	I_{rel} (%)
788.4256(3)	788.4328 (3+) → 0 (2+)	14700	100
1164.860(1)	1164.8799 (1+) → 0 (2+)	6900	100
1601.065(3)	1601.1034 (1+) → 0 (2+)	640	100
1951.1265(1)	1951.1853 (2-) → 0 (2+)	1870	100
1959.337(1)	1959.394 (2+) → 0 (2+)	43.6	100
517.07(3)	2468.26 (3+) → 1951.18 (2-)	970	100
1327.396(1)	2492.303 (3+) → 0 (2+)	40	100
2518.301(3)	2518.396 (3+) → 0 (2+)	1610	100
2676.323(3)	2676.440 (3+) → 0 (2+)	21	100

(1) Identified in the spectrum
(2) Supposedly present but interfered by more intense peaks or masked in the continuum
(3) Unobserved

broadening. The *a priori* unbroadened 1552-keV peak might be merged with the 1554-keV peak due to ^{19}F(α, n)^{22}Na, as reported earlier. The excited ^{30}Si levels can be produced by inelastic scattering of neutrons or alpha particles, silicon being a major chemical element in the waste with a ^{30}Si isotopic abundance of 3%. It can also be produced by (α, p) reaction on ^{27}Al.

14) Four gamma rays corresponding to de-excitation of ^{36}Cl nuclei produced by neutron radiative capture on ^{35}Cl (76% abundance in chlorine and large cross section of 43.6 b [18]) are identified in the spectrum, as reported in Table IX [32]. The 788- and 517-keV gamma rays are probably masked by the intense americium and plutonium signal. The 1601 keV (very close to the intense 1592-keV peak of ^{208}Tl), 2518 keV (maybe masked by the 2510.01-keV Doppler broadened peak due to ^{23}Na(α, p)^{26}Mg), and 2676 keV (large Doppler broadening expected due to the short lifetime of the excited level, 21 fs) are also not visible.
15) The 847-keV transition between first excited level and ground state of ^{56}Fe is identified in the spectrum, as well as the 1238-keV transition between its two and one excited levels [33]. The high atomic number of iron does not allow alpha particles to get through the Coulomb barrier, so neutron inelastic scattering on ^{56}Fe is the main reaction responsible for these two gamma rays. In addition to the neutron and gamma correlation in the (n, n′) reaction, the cascade between the 1238- and 847-keV gamma rays can lead to the emission of up to three time-correlated particles, potentially leading to high order parasitical coincidences with respect to plutonium spontaneous fission coincidences.

C. 4000–6400-keV Region of Interest

The high-energy region of the spectrum in Fig. 5 shows neutron-induced radiative capture and inelastic scattering gamma rays on carbon and oxygen nuclei (see Table X) that are present inside the waste drum. The 4946.31-keV radiative capture gamma ray on ^{12}C nuclei is weak but present, as well as the 6128.63-keV inelastic scattering gamma ray on ^{16}O accompanied by its SE and DE peaks. The ^{16}O(n, n′) reaction may also lead to 6917- and 7117-keV gamma rays [17] but they are beyond the 6400-keV end-energy of the spectrum. After a discussion with the detector manufacturer, the artifact peak near 5500 keV is probably due to a connection issue of the "energy" cable between the preamplifier and the digital

TABLE X
PEAK ENERGIES AND BRANCHING RATIO IN 4000–6400-keV RANGE

Original nuclide	Energy (keV)	Intensity (%) or Cross section (mbarn)	Reaction or radioactive daughter
^{12}C	4946.31	3.53 mb	(n,γ) ^{13}C
^{16}O	5106.63	-	DE 6128.63
^{16}O	5617.63	-	SE 6128.63
^{16}O	6128.63	148 mb	(n,n') ^{16}O

electronics. This peak was also present in the background noise spectrum. It is important to note that some peaks of this region remain to be identified (e.g., near 4700 and 5500 keV).

IV. CONCLUSION

The detailed gamma-ray spectrometry analysis of a 120-L waste drum filled with plutonium bearing glove box filters allowed us to identify, besides natural background gamma and X-rays (^{40}K, U, and Th chains) and well-known gamma and X-rays due to plutonium and americium radioactive decays, a number of less common gamma rays. These remaining rays are due to nuclear (α, x) reactions induced by the high alpha activity of Pu and Am, as well as by neutrons from spontaneous fissions and (α, n) reactions. The analysis of the residual nuclei excited levels produced in alpha- and neutron-induced reactions allowed us to identify several unusual gamma rays and the potential spurious coincidences that they could produce in a neutron multiplicity measurement system with plastic scintillators. The observed lines, as well as the Maxwellian distribution of spontaneous fission neutrons, will be used in further Monte Carlo N-Particles (Transport Code) (MCNP) simulations to compare pulse-height spectra of energies deposited by neutrons and gamma rays in plastic scintillators. It will allow us to estimate the interest of placing low- and high-energy rejection thresholds to limit the influence of parasitic coincidence involving gamma rays.

REFERENCES

[1] R. Kouzes *et al.*, "Neutron detection alternatives to ^{3}He for national security applications," *Nucl. Instrum. Methods Phys. Res. A, Accel. Spectrom. Detect. Assoc. Equip.*, vol. 623, pp. 1035–1045, Jan. 2010.

[2] D. Henzlova *et al.*, "Current status of ^{3}He alternatives technologies for nuclear safeguards," Los Alamos Nat. Lab., New Mexico, NM, USA, Tech. Rep. LA-UR-15-21201 Ver. 3, PNNL-24307, Jul. 2015.

[3] B. Simony *et al.*, "Cross-talk characterization in passive neutron coincidence counting of radioactive waste drums with plastic scintillators," *IEEE Trans. Nucl. Sci.*, vol. 63, no. 3, pp. 1513–1519, Jun. 2016.

[4] B. Simony *et al.*, "Passive neutron coincidence counting with plastic scintillators for the characterization of radioactive waste drums," *IEEE Trans. Nucl. Sci.*, vol. 64, no. 10, pp. 2719–2724, Oct. 2017.

[5] S. A. Pozzi, S. D. Clarke, M. Flaska, and P. Peerani, "Pulse-height distributions of neutron and gamma rays from plutonium-oxide samples," *Nucl. Instrum. Meth. Phys. Res. A, Accel. Spectrom. Detect. Assoc. Equip.*, vol. 608, pp. 310–315, Sep. 2009.

[6] A. C. Kaplan, M. Flaska, A. Enqvist, J. L. Dolan, and S. A. Pozzi, "EJ-309 pulse shape discrimination performance with a high gamma-ray-to-neutron ratio and low threshold," *Nucl. Instrum. Meth. Phys. Res. A, Accel. Spectrom. Detect. Assoc. Equip.*, vol. 729, pp. 463–468, Nov. 2013.

[7] A. Di Fulvio *et al.*, "Passive assay of plutonium metal plates using a fast-neutron multiplicity counter," *Nucl. Instrum. Meth. Phys. Res. A, Accel. Spectrom. Detect. Assoc. Equip.*, vol. 855, pp. 92–101, May 2017.

[8] N. Zaitseva *et al.*, "Plastic scintillators with efficient neutron/gamma pulse shape discrimination," *Nucl. Instrum. Meth. Phys. Res. A, Accel. Spectrom. Detect. Assoc. Equip.*, vol. 668, pp. 88–93, Mar. 2012.

[9] G. H. V. Bertrand, M. Hamel, S. Normand, and F. Sguerra, "Pulse shape discrimination between (fast or thermal) neutrons and gamma rays with plastic scintillators: State of the art," *Nucl. Instrum. Meth. Phys. Res. A, Accel. Spectrom. Detect. Assoc. Equip.*, vol. 776, pp. 114–128, Mar. 2015.

[10] R. S. Woolf, A. L. Hutcheson, C. Gwon, B. F. Phlips, and E. A. Wulf, "Comparing the response of PSD-capable plastic scintillator to standard liquid scintillator," *Nucl. Instrum. Meth. Phys. Res. A, Accel. Spectrom. Detect. Assoc. Equip.*, vol. 784, pp. 80–87, Jun. 2015.

[11] M. P. Taggart and P. J. Sellin, "Comparison of the pulse shape discrimination performance of plastic scintillators coupled to a SiPM," *Nucl. Instrum. Meth. Phys. Res. A, Accel. Spectrom. Detect. Assoc. Equip.*, vol. 908, pp. 148–153, Nov. 2018.

[12] C. Carasco, B. Pérot, S. Normand, and G. Sannié, "POLITRANI, a new toolkit to simulate organic scintillator pulses," *IEEE Trans. Nucl. Sci.*, vol. 61, no. 4, pp. 2071–2074, Aug. 2014.

[13] G. Corre, K. Boudergui, G. Sannié, and V. Kondrasovs, "Neutron detection with large plastic scintillators for RPM applications," in *Proc. 4th Int. Conf. Advancements Nucl. Instrum. Meas. Meth. Appl. (ANIMMA)*, Lisbon, Portugal, Apr. 2015, pp. 1–4.

[14] T. E. Sampson, "Plutonium isotopic composition by gamma-ray spectroscopy, a review," Los Alamos Nat. Lab., New Mexico, NM, USA, Tech. Rep. LA-10750-MS, Sep. 1986.

[15] *ENSDF, Evaluated Nuclear Structured Data File Search and Retrieval*. Accessed: Mar./Jul. 2019. [Online]. Available: https://www.nndc.bnl.gov/ensdf/

[16] *EMPIRE-II Version 2.18 (Mondovi)*. Accessed: Jan. 2019. [Online]. Available: https://www-nds.iaea.org/empire218/

[17] S. P. Simakov, A. Pavlik, H. Vonach, and S. Hlavac, "Status of experimental and evaluated discrete gamma-ray production at $E_n = 14.5$ MeV," Int. Nucl. Data Committee, Vienna, Austria, Final Rep. INDC(CCP)-413, Sep. 1998.

[18] R. B. Firestone *et al.*, *Database of Prompt Gamma Rays From Slow Neutrons Capture for Elemental Analysis*. Vienna, Austria: IAEA, 2006, pp. 55–68 and 94–158.

[19] F. Ajzenberg-Selove, "Energy levels of light nuclei A=13–15*," *Nucl. Phys. A*, vol. 523, pp. 1–196, Feb. 1991.

[20] J. F. Ziegler, M. D. Ziegler, and J. P. Biersack, "SRIM—The stopping and range of ions in matter (2010)," *Nucl. Instrum. Meth. Phys. Res. B, Beam Interact. Mater. At.*, vol. 268, nos. 11–12, pp. 1818–1823, Jun. 2010.

[21] D. R. Tilley, H. R. Weller, and C. M. Cheves, "Energy levels of light nuclei A=16–17*," *Nucl. Phys. A*, vol. 565, no. 1, pp. 1–184, Nov. 1993.

[22] C. Carasco *et al.*, "Material characterization in cemented radioactive waste with the associated particle technique," *Nucl. Instrum. Methods Phys. Res. A, Accel. Spectrom. Detect. Assoc. Equip.*, vol. 619, nos. 1–3, pp. 432–435, Jul. 2010.

[23] D. R. Tilley, H. R. Weller, C. M. Cheves, and R. M. Chesteler, "Energy levels of light nuclei A=18–19*," *Nucl. Phys. A*, vol. 595, no. 1, pp. 1–170, Dec. 1995.

[24] R. B. Firestone, "Nuclear data sheets for A=21," *Nucl. Data Sheets*, vol. 127, pp. 1–68, Jul./Aug. 2015.

[25] M. S. Basunia, "Nuclear data sheets for A=22," *Nucl. Data Sheets*, vol. 127, pp. 69–190, Jul./Aug. 2015.

[26] R. B. Firestone, "Nuclear data sheets for A=25," *Nucl. Data Sheets*, vol. 110, no. 8, pp. 1691–1744, Aug. 2009.

[27] M. S. Basunia and A. M. Hurst, "Nuclear data sheets for A=26," *Nucl. Data Sheets*, vol. 134, pp. 1–148, May/Jun. 2016.

[28] M. S. Basunia, "Nuclear data sheets for A=27," *Nucl. Data Sheets*, vol. 112, no. 8, pp. 1875–1948, Aug. 2011.

[29] M. S. Basunia, "Nuclear data sheets for A=28," *Nucl. Data Sheets*, vol. 114, no. 10, pp. 1189–1291, Oct. 2013.

[30] M. S. Basunia, "Nuclear data sheets for A=29," *Nucl. Data Sheets*, vol. 113, no. 4, pp. 909–972, Apr. 2012.

[31] M. S. Basunia, "Nuclear data sheets for A=30," *Nucl. Data Sheets*, vol. 111, no. 9, pp. 2331–2424, Sep. 2010.

[32] N. Nica, "Nuclear data sheets for A=36," *Nucl. Data Sheets*, vol. 113, no. 1, pp. 1–155, Jan. 2012.

[33] H. Junde, "Nuclear data sheets for A=56," *Nucl. Data Sheets*, vol. 112, no. 6, pp. 1513–1645, Jun. 2011.